Critical flow and clustering in a model of granular transport: The interplay between drift and antidiffusion

Giorgos Kanellopoulos and Ko van der Weele
Mathematics Department, University of Patras, 26500 Patras, Greece
(Received 28 December 2011; published 5 June 2012)

We study the transport of granular matter through a staircaselike array of K vertically vibrated compartments. Given a constant inflow rate $Q < Q_{\rm cr}(K)$ into the top compartment, a continuous particle flow establishes itself along the entire length of the system. However, as soon as Q grows beyond the critical value $Q_{\rm cr}(K)$ the particles form a cluster and the flow comes to a halt. Interestingly, this clustering is preceded by a subcritical warning signal: for Q values just below $Q_{\rm cr}(K)$ the density profile along the conveyor belt spontaneously develops a pattern in which the compartments are alternatingly densely and sparsely populated. In a previous paper [Kanellopoulos and van der Weele, Int. J. Bifurcation Chaos **21**, 2305 (2011)] this pattern was shown to be the result of a period-doubling bifurcation. The present paper aims at unravelling the *physical* mechanism that lies at the basis of the pattern formation. To this end we study the continuum version of the same system, replacing the compartment number $k = 1, \ldots, K$ by a continuous variable x. The dynamics of the system is now described (instead of by K coupled ordinary differential equations) by a single *partial* differential equation of the Fokker-Planck type, with a drift and a diffusive term that both depend on the density. The drift term turns out to be responsible for the subcritical density oscillations, thereby paving the way for the eventual clustering which sets in when the diffusion coefficient becomes negative. The observed sequence of events in the granular transport system is thus explained as an interplay between drift and (anti)diffusion.

DOI: 10.1103/PhysRevE.85.061303 PACS number(s): 45.70.Qj, 05.60.Cd, 02.60.Lj

I. INTRODUCTION

The flow of granular materials is a subject that has attracted a great deal of interest during the past decade, both from a practical and from a fundamental point of view. Particle flows are encountered in countless instances ranging from the smooth sand stream in an hourglass to devastating rock avalanches in mountainous regions [1–6]. In industry and agriculture, granular materials are so ubiquitous that it has been estimated that no less than 10% of the global energy budget is spent on the transport and handling of them [7,8]. From the fundamental side, granular flows are among the most readily accessible examples of multiparticle systems far from equilibrium, ideally suited for studying collective dynamical effects and spontaneous pattern formation [9–12]. For this reason, the results of the present study are not only relevant for granular materials but also have bearing on related multiparticle flows such as vehicle traffic on highways, pedestrian crowds rushing toward emergency exits, or ant trails [13–15].

Here we study the flow of granular material though the transport system depicted in Fig. 1. It consists of an array of connected compartments $k = 1, \ldots, K$, vibrated vertically, with particles being inserted into the first compartment and exiting from the last. The flow inside the system is modelled by flux functions: the number of particles that leave compartment k per unit time in the downstream direction is given by a flux function $F_R(n_k)$, and in the upstream direction by a smaller function $F_L(n_k)$. These flux functions depend on $n_k(t)$, the normalized number of particles in the compartment, in a nonmonotonic way: starting out from zero particles per second at $n_k = 0$, the flux does *not* grow indefinitely but attains a maximum at some intermediate value of n_k, and beyond this value decreases again. This is a consequence of the fact that the particles do not collide elastically. They lose a small portion of their kinetic energy in every collision, so they collectively make each other less mobile, an effect which is especially strong when there are many particles in the compartment.

Indeed, this dissipation of energy is one of the most characteristic features of a granular gas and the one that makes it fundamentally different from any ordinary molecular gas. It is the reason why the granular particles tend to cluster together, forming patterns of dense and dilute regions, whereas the molecules in a normal gas do exactly the opposite and occupy the space available to them in a uniform fashion. When the particle density in one of the compartments exceeds a certain critical threshold value (depending on the shaking strength, the steepness of the staircase, and other factors to be discussed below) the clustering becomes irreversible and the particle flow is not able to get past this compartment anymore.

In the present paper we will work with the following approximate flux functions, illustrated in Fig. 2 [16–20]:

$$F_{R,L}(n_k) = A n_k^2 e^{-B_{R,L} n_k^2}. \tag{1}$$

The indices R and L denote the flow toward the right and left, respectively, and $n_k(t)$ represents the (normalized) number of particles in the kth compartment.

The above form of the flux function was first derived by Eggers [16] (see also [21–23]), treating the particles inside the compartment as a dissipative gas under various simplifying assumptions. For instance, the particles are assumed to obey the ideal-gas law (relating the particle density in the compartment to the pressure and granular temperature) and to lose energy only in the collisions between themselves, but not in those with the walls of the compartment. It is to be regarded as a minimal model, capturing the essence of the matter rather than aiming at a precise quantitative agreement. The simplifying assumptions can in principle all be refined, but in that case the analytical approximation Eq. (1) will be replaced

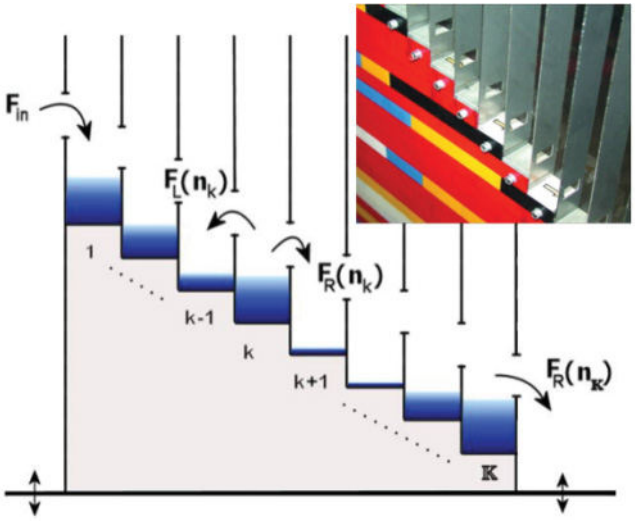

FIG. 1. (Color online) Model conveyor belt consisting of K compartments, vertically vibrated to make the granular particles mobile. Material from the kth compartment is able to flow into either of its neighboring compartments: The flow to box $k-1$ is prescribed by a flux function $F_L(n_k)$ and that to box $k+1$ by a somewhat larger flux function $F_R(n_k)$. The adjustable inflow rate into the top compartment is denoted by F_{in}. Under standard operating conditions the outflow rate from the last compartment, $F_R(n_K)$, will be equal to the inflow rate F_{in}. The inset shows an experimental realization of the system.

by a much more cumbersome numerical expression. In the present work we will stick to Eggers' form of the flux function.

The number density $n_k(t)$ is taken to be a continuous quantity, which is a reasonable approximation as long as there are sufficiently many particles in each compartment. The total number of particles in the system is generally not conserved, since there is an inflow of particles in the first compartment and an outflow from the last one. Only under steady operating conditions (when the outflow equals the inflow) will the total number of particles be constant.

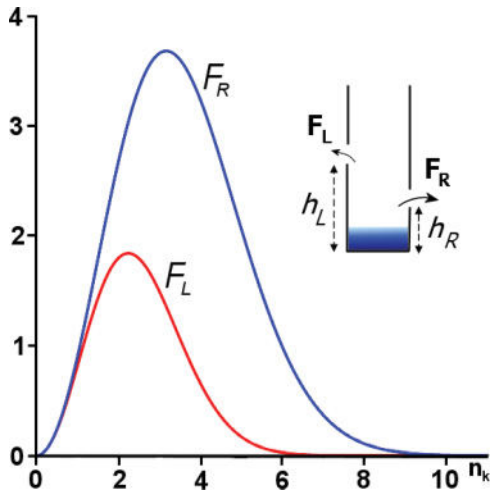

FIG. 2. (Color online) The flux functions $F_R(n_k)$ (with $B_R = 0.1$) and $F_L(n_k)$ (with $B_L = 0.2$) used in the text. The barrier to the right is twice as low as that to the left, hence the particle flux toward the right is considerably larger.

The prefactor A determines the absolute scale of the flow rate and, having dimensions s^{-1}, may be used to nondimensionalize the time variable. That is, one may work with the nondimensional time variable $\tau = At$.

The dimensionless parameter $B_{R,L}$ is proportional to Refs. [21,22]

$$B_{R,L} \propto \frac{g h_{R,L}}{(af)^2}(1-\eta^2)^2, \tag{2}$$

where $g = 9.81\ \text{m/s}^2$ is the gravitational acceleration, $h_{R,L}$ is the height of the barrier toward the neighboring compartments at the right and the left, respectively, a and f are the amplitude and frequency of the sinusoidal driving signal, and η is the effective coefficient of restitution of the particle-particle collisions. A typical value of η, measured experimentally for spherical glass particles of 2 mm diameter, is 0.95, meaning that $(1-\eta^2)^2 \approx 0.01$. For perfectly elastic collisions the value of η would be 1, i.e., $(1-\eta^2)^2 = 0$, so in that case B_R and B_L would be identically zero; the flux functions given by Eq. (1) would then take the monotonically increasing form $F_{R,L}(n_k) = An_k^2$ and clustering would not be possible.

In the present context reasonable values are $B_R = 0.1$ and $B_L = 0.2$, which means that the height of the barrier toward the right (h_R) is taken to be twice as low as h_L. The functions $F_R(n_k)$ and $F_L(n_k)$ with these choices of $B_{R,L}$ are depicted in Fig. 2. They are the same as in our earlier work [20], enabling a direct comparison of the results.

Given the above flux functions, and a controllable influx $F_{\text{in}}(\tau)$ into the first compartment, the time evolution of the system is governed by the following system of K coupled ordinary differential equations (with the dimensionless time variable $\tau = At$):

$$\begin{aligned}
\frac{dn_1}{d\tau} &= F_{\text{in}}(\tau) - F_R(n_1) + F_L(n_2) \quad \text{for } k = 1,\\
\frac{dn_k}{d\tau} &= F_R(n_{k-1}) - F_L(n_k) - F_R(n_k) + F_L(n_{k+1})\\
&\qquad\qquad \text{for} \quad k = 2,\ldots,K-1,\\
\frac{dn_K}{d\tau} &= F_R(n_{K-1}) - F_L(n_K) - F_R(n_K)\\
&\qquad\qquad \text{for} \quad k = K.
\end{aligned} \tag{3}$$

These equations express the mass balance for each compartment: The change in the density $n_k(\tau)$ per unit time is equal to the inflow rate into this compartment minus the outflow rate. In the present work we will restrict ourselves to time-independent inflow rates into the first compartment, $F_{\text{in}}(\tau) = Q$. The flow that this induces in the rest of the system is found by numerically solving the set of equations (3).

The above model does not take into account statistical fluctuations around the behavior dictated by the flux functions. Instead, it is a mean-field model representing the average behavior of a sufficiently large number of experimental realizations. The influence of fluctuations could be incorporated by adding a stochastic noise term to the equations (see, e.g., the original paper by Eggers [16], worked out in detail in Ref. [24]) or alternatively by an urn model approach in the spirit of Lipowski and Droz [25–27].

II. BRIEF REVIEW OF THE CLUSTER TRANSITION IN THE DISCRETE SYSTEM

To get an impression of what the solution of Eq. (3) looks like, we focus here on a representative case with $K = 155$ compartments. This is a sufficiently large number to give an accurate comparison with the continuum model of the next sections. In fact, any number $K \gtrsim 20$ would be sufficient for a meaningful comparison with the continuum limit of $K \to \infty$, as we have shown in a previous study [20].

Let us start with a uniform density profile $n_k(0) = 1$ for all $k = 1, \ldots, K$ and apply a small, steady inflow rate $F_{\text{in}}(\tau) = Q = 1.00$. This value of Q is well below the maximum capacity of the conveyor belt. The material will therefore flow smoothly downward and after a while a dynamical equilibrium is established along the entire length of the system. From that moment, the density profile does not change anymore ($dn_k/d\tau = 0$ for all k): The equilibrium profile is shown in Fig. 3(a). We see that n_k is at a constant level 2.09 along the whole system except for a sharp drop at the end. For future reference we note that the slope here is -0.53 density units per compartment. The level of the last compartment in the steady state is found from $F_R(n_K) = Q$, which can be solved analytically [20].

Now we gradually increase the inflow rate, in very small steps, taking care that in each step the system gets enough time to adapt to the new Q value and settle in its new equilibrium state. At $Q = 1.80$ the level has risen to $n_k = 2.68$ and, more importantly, a disturbance in the form of a density oscillation is seen to break the uniformity of the profile [Fig. 3(b)]. This oscillation (the first signs of which emerge already around $Q = 1.50$, when the density level is at 2.46 and the negative slope at the right end equals -0.75) originates at the far end of the system and has a marked periodicity of two compartments.

As we increase the inflow rate further the oscillatory pattern spreads toward the left, resembling a zipper that is being opened. At $Q = 1.87$ [Fig. 3(c)] the oscillations have proceeded up to compartment $k \approx 80$, and at the critical value $Q_{\text{cr}} = 1.873\,467\,53$ [Fig. 3(d)] the oscillations have covered the entire length of the system in a homogeneous way. The density goes up and down between the values 3.013 and 2.505, and the slope at the right end equals -0.99. Here we have reached the maximum capacity of the system. Any further increase of Q will lead to the formation of a cluster and the obstruction of the flow [28].

To illustrate this, Fig. 4 shows what happens when, starting out from the state of Fig. 3(d), we apply an inflow $Q = 1.874\,00 > Q_{\text{cr}}$. After 600 time steps the density of the first compartment is seen to grow rapidly, meaning that the system is no longer able to transfer the incoming material toward the right. Instead, the particles entering the conveyor belt are now immediately trapped in the first compartment, where the surplus of material grows and grows and a cluster is formed. To make matters worse, every new particle adds to the efficiency of the trap by increasing the number of inelastic collisions in this compartment. Meanwhile, the material in the remaining compartments gradually flows out of the system. In the first instance it does so in the form of a shock wave with a well-recognizable front [19]; later, when less material is involved in the flow, the profile takes a more symmetric shape.

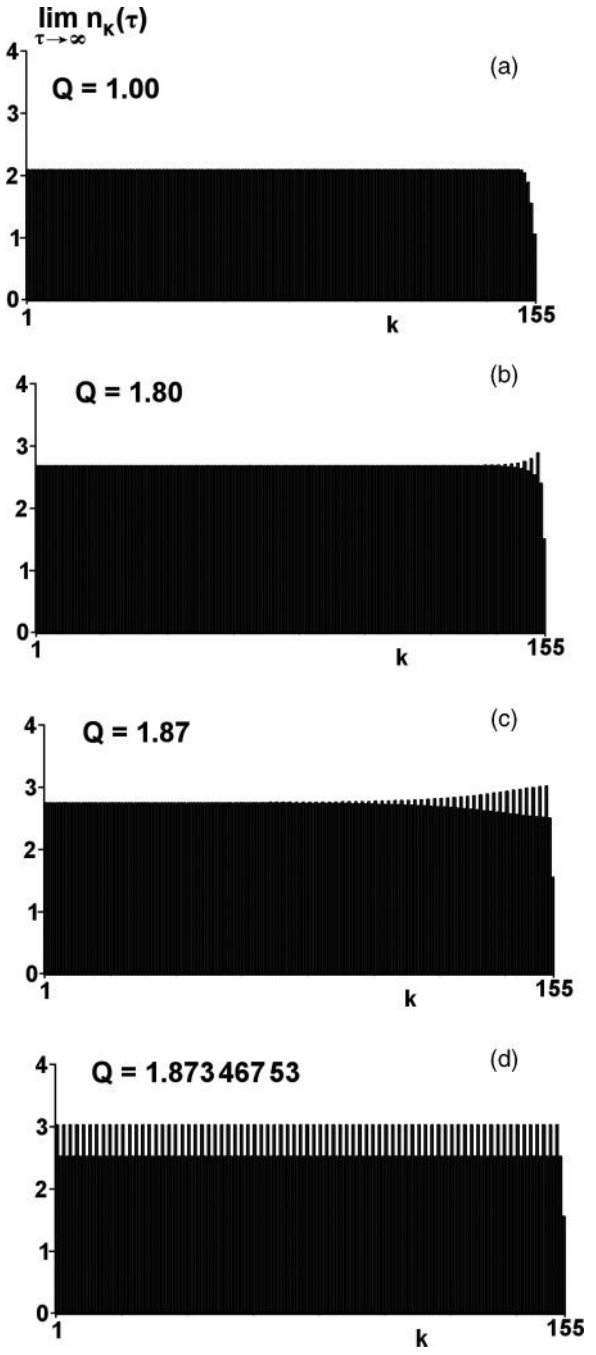

FIG. 3. (a) The density profile (under steady flow conditions) for $Q = 1.00$ in a conveyor belt consisting of 155 compartments. In the next plots we gradually increase the inflow rate, each time giving the system enough time to adapt to the new Q value, so all depicted profiles represent dynamical equilibrium states in which the outflow equals the inflow. (b) At $Q = 1.80$ an oscillatory pattern appears at the right hand side of the system. (c) A further increase of the inflow rate to $Q = 1.87$ causes the wavy pattern to expand toward the left. (d) At $Q = Q_{\text{cr}} = 1.873\,467\,53$ the amplitude of the oscillation becomes uniform along the entire length of the system, meaning that the maximum capacity of the conveyor belt has been reached.

This is connected to the fact that $F_R[n_k(\tau)]$ and $F_L[n_k(\tau)]$ become practically indistinguishable when the density $n_k(\tau)$ goes to zero.

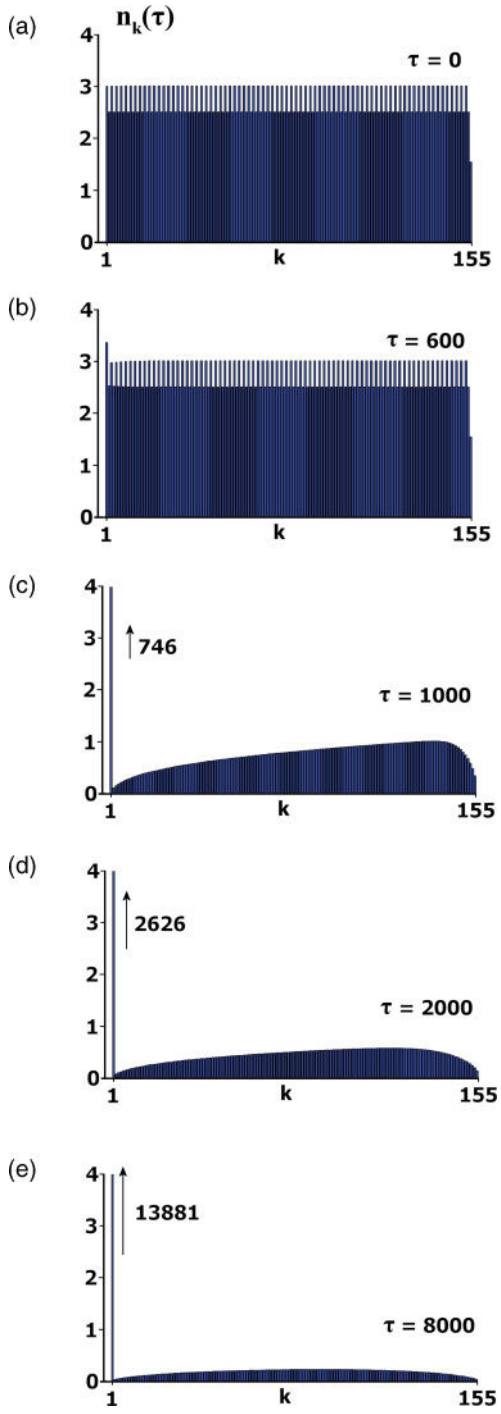

FIG. 4. (Color online) Breakdown of the granular flow in five snapshots. Starting from the oscillatory profile of Fig. 3(d), at $\tau = 0$ we increase the inflow rate to $Q = 1.8740$, i.e., beyond the critical value $Q_{\rm cr}$. We witness the formation of a cluster in the first compartment, capturing all incoming particles and obstructing the flow. The remaining material in the other compartments still travels to the right but once this has flown out of the system the transport comes to a complete halt. (a) $\tau = 0$, (b) $\tau = 600$, (c) $\tau = 1000$, (d) $\tau = 2000$, (e) $\tau = 8000$. In all these plots the vertical axis has been shifted a bit toward the left in order to show the cluster more clearly.

In the above sequence of events we distinguish two key steps. The *first* step is when the density oscillations appear at the end of the system around $Q = 1.50$. The throughput is still unaffected, yet these oscillations are a warning signal that the maximum capacity of the conveyor belt is almost reached. The *second* step comes at $Q = Q_{\rm cr} = 1.873\,467\,53$, when the oscillatory pattern has covered the entire length of the system and a cluster is about to be formed in the top compartment.

In the above theory, the density $n_1(t)$ in the first compartment will tend to infinity (see Fig. 4); in practice this means that the compartment will burst and it is clearly advisable to turn off the conveyor belt before it comes to that. The reader may wonder how the scenario changes if the compartments are able to hold only a finite amount of material, say $n_{\rm full} = 10.0$, and start to flow over (through the opening downward) as soon as this threshold is exceeded.

Since the above value of $n_{\rm full}$ is well above the critical value $n = B_R^{-1/2} = 3.162$ for which the clustering sets in [20], this change in the model does not in any way affect the precluster stages. So up to the stage of Fig. 4(b) ($\tau = 600$) everything will occur in exactly the same way. It is only *after* the clustering has set in that the system starts to behave differently: When the first compartment is filled to $n_{\rm full}$, it flows over into the second compartment. And when the second compartment in turn is filled to the brim, it flows over into the third compartment, and so on. The final state of affairs is that all compartments are filled to the maximum level $n_{\rm full}$ [with the exception of the last compartment, which settles in the inflow-rate dependent level $n_K(Q)$ given by $F_R(n_K) = Q$] and the granular material that enters the system, instead of getting stuck in the first compartment, now flows smoothly—and quite efficiently!—from one compartment to the next, not unlike the constant flow of water through the successive basins of a cascade fountain.

The only thing that limits the efficiency of the granular cascade, and sets an upper bound to the amount of material that can be transported per unit time, is the finite size of the openings between the compartments. If one pushes the inflow rate beyond this upper bound, the extra material will again heap up in the first compartment, just as in the system without overflow.

For our purposes (i.e., the study of the subcritical phenomena *preceding* the clustering) the two models are completely equivalent. In the remainder of this paper we will therefore continue to study the model *without* overflow.

III. CONTINUUM VERSION OF THE FLUX MODEL

In order to understand the physics behind the breakdown of the flow and the cluster formation, we study the continuum version of the flux model described in Eqs. (1)–(3). In the continuum description, the discrete position variable k (indicating the compartments $k = 1, \ldots, K$) is replaced by a continuous variable x. Correspondingly, the fraction $n_k(t)$ is replaced by $\rho(x,t)\Delta x$, where $\rho(x,t)$ is the number density per unit length and Δx the width of a compartment [19,29].

This replacement of $n_k(t)$ by $\rho(x,t)\Delta x$ transforms the flux functions $F_{L,R}[n_k(t)]$ into their continuum counterparts $\widetilde{F}_{L,R}(\rho(x,t))$ as follows:

$$\widetilde{F}_{L,R}(\rho(x,t)) = \frac{1}{\Delta x} F_{L,R}(\rho(x,t)\Delta x), \tag{4}$$

where we note that the dimensionality of the original flux functions $F_{L,R}[n_k(t)]$ is number of particles per unit time, no./s, whereas that of $\widetilde{F}_{L,R}(\rho(x,t))$ is number *density* per unit time, i.e., (no./m)/s. In the particular case of the Eggers flux function Eq. (1), the continuum expression (4) takes the following form:

$$\widetilde{F}_{R,L}(\rho(x,t)) = A\Delta x\rho^2 e^{-B_{R,L}\Delta x^2\rho^2}. \tag{5}$$

and, as before, this may be turned into dimensionless form by using dimensionless variables $\tau = At$ and $\xi = x/\Delta x$ (meaning that ξ runs from 0 to K). We will come back to this later.

Using Eq. (4), the balance equation Eq. (3) becomes [19]

$$\begin{aligned}\frac{\partial\rho(x,t)}{\partial t} &= \widetilde{F}_R(\rho(x-\Delta x,t)) - \widetilde{F}_R(\rho(x,t)) \\ &\quad - \widetilde{F}_L(\rho(x,t)) + \widetilde{F}_L(\rho(x+\Delta x,t)) \\ &= -\Delta x\left(\frac{\partial\widetilde{F}_R}{\partial x} - \frac{\partial\widetilde{F}_L}{\partial x}\right) \\ &\quad + \frac{1}{2}(\Delta x)^2\left(\frac{\partial^2\widetilde{F}_R}{\partial x^2} + \frac{\partial^2\widetilde{F}_L}{\partial x^2}\right) + \cdots,\end{aligned} \tag{6}$$

where the second step follows from a Taylor expansion up to second order in Δx. Using the chain rule for partial differentiation [$\partial\widetilde{F}_R/\partial x = (d\widetilde{F}_R/d\rho)(\partial\rho/\partial x)$, etc.] the above equation can also be written as

$$\frac{\partial\rho}{\partial t} = -P(\rho)\frac{\partial\rho}{\partial x} + \frac{\partial}{\partial x}\left\{D(\rho)\frac{\partial\rho}{\partial x}\right\}, \tag{7}$$

with the coefficients $P(\rho)$ and $D(\rho)$ given by

$$P(\rho) = \Delta x\left(\frac{d\widetilde{F}_R}{d\rho} - \frac{d\widetilde{F}_L}{d\rho}\right), \tag{8}$$

$$D(\rho) = \frac{1}{2}\Delta x^2\left(\frac{d\widetilde{F}_R}{d\rho} + \frac{d\widetilde{F}_L}{d\rho}\right). \tag{9}$$

Equation (7) is the continuum counterpart of the balance equation (3). It is a second-order partial differential equation of parabolic type. The right hand side contains a drift term, with density-dependent *drift velocity* $P(\rho)$, and a diffusion term with density-dependent *diffusion coefficient* $D(\rho)$. Its general appearance resembles the famous Fokker-Planck equation from the theory of stochastic processes [30–32]. They differ, however, in the structure of the diffusion term. In the Fokker-Planck equation this term has the form $\partial^2/\partial x^2\{D(x,t)\rho(x,t)\}$, which means that the two equations coincide only when D is independent of x. This is not the case in the present paper.

It is perhaps good to stress straight away that the above continuum model is an *approximation* to the discrete system. To obtain a complete correspondence one would have to include all higher orders in the Taylor expansion in Eq. (6). Obviously this is not our goal, but it means that we willingly accept small deviations from the discrete system as a consequence of these neglected higher-order terms in the continuum model. It will turn out that these deviations are indeed small, and that Eq. (7) captures all the main features of the clustering transition, including the oscillatory profile.

Especially this latter point is worth emphasizing, since intuitively one might expect a continuum model to be capable of describing only the global features of the dynamics (not the local ones) and this would exclude any oscillations with a wavelength comparable to the discreteness of the system. The present continuum model, however, is perfectly able to reproduce the subcritical oscillations since it has been derived from the original discrete system on precisely the right level of detail (the step size in the Taylor expansion was chosen to be Δx). In passing we note that we have not included a noise term in the partial differential equation (7), so just as in the discrete system we are aiming at a mean-field description of the dynamics.

In the case of the Eggers-type flux functions $\widetilde{F}_{R,L}(\rho)$ given by Eq. (5), the coefficients $P(\rho)$ and $D(\rho)$ have the following specific form:

$$\begin{aligned}P(\rho) = 2A(\Delta x)^2\rho\{&[1 - B_R(\Delta x)^2\rho^2]e^{-B_R(\Delta x)^2\rho^2} \\ &- [1 - B_L(\Delta x)^2\rho^2]e^{-B_L(\Delta x)^2\rho^2}\},\end{aligned} \tag{10}$$

$$\begin{aligned}D(\rho) = A(\Delta x)^3\rho\{&[1 - B_R(\Delta x)^2\rho^2]e^{-B_R(\Delta x)^2\rho^2} \\ &+ [1 - B_L(\Delta x)^2\rho^2]e^{-B_L(\Delta x)^2\rho^2}\},\end{aligned} \tag{11}$$

which are depicted in Fig. 5(b). We observe that both the drift velocity $P(\rho)$ (with which density perturbations travel through the system) and the diffusion coefficient $D(\rho)$ (which determines whether a density disturbance will be smoothed out or not) are positive for small values of ρ but become *negative* at larger densities. This will play a crucial role in the explanation of the clustering transition.

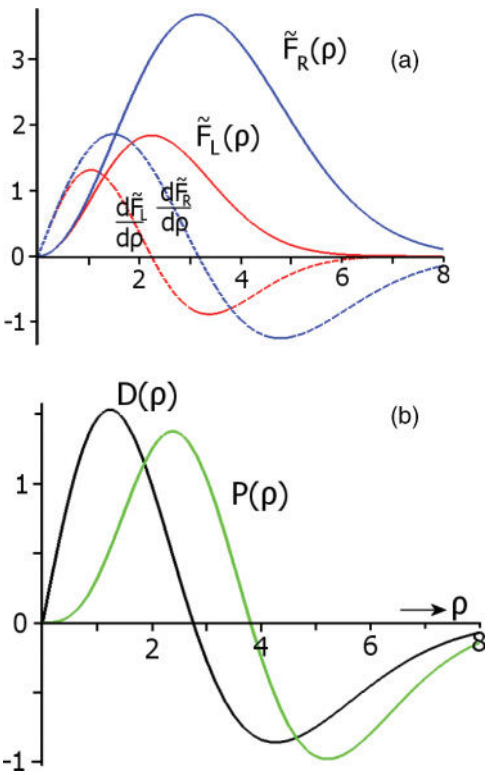

FIG. 5. (Color online) (a) The flux functions $\widetilde{F}_R(\rho)$ and $\widetilde{F}_L(\rho)$ given by Eq. (5) for $A = 1\ \mathrm{s}^{-1}$, $\Delta x = 1$ m, $B_R = 0.1$, and $B_L = 0.2$. Also shown (as dashed curves) are their derivatives $d\widetilde{F}_R/d\rho$ and $d\widetilde{F}_L/d\rho$. (b) The corresponding drift velocity $P(\rho)$ and diffusion coefficient $D(\rho)$, given by Eqs. (8)–(11).

As noted before, the problem can also be cast in dimensionless form. With the transformations $x \to \xi = x/\Delta x$, $t \to \tau = At$, and $\rho(x,t) \to \widetilde{\rho}(\xi,\tau) = \rho(x,t)\Delta x$ the drift-diffusion equation [with the drift and diffusion coefficients based on the Eggers flux function, as in Eqs. (10) and (11)] takes the form

$$\frac{\partial \widetilde{\rho}}{\partial \tau} = -\widetilde{P}(\widetilde{\rho})\frac{\partial \widetilde{\rho}}{\partial \xi} + \frac{\partial}{\partial \xi}\left\{\widetilde{D}(\widetilde{\rho})\frac{\partial \widetilde{\rho}}{\partial \xi}\right\} \tag{12}$$

with

$$\widetilde{P}(\widetilde{\rho}) = 2\widetilde{\rho}[(1 - B_R\widetilde{\rho}^2)e^{-B_R\widetilde{\rho}^2} - (1 - B_L\widetilde{\rho}^2)e^{-B_L\widetilde{\rho}^2}] \tag{13}$$

and

$$\widetilde{D}(\widetilde{\rho}) = \widetilde{\rho}[(1 - B_R\widetilde{\rho}^2)e^{-B_R\widetilde{\rho}^2} + (1 - B_L\widetilde{\rho}^2)e^{-B_L\widetilde{\rho}^2}]. \tag{14}$$

We will work with this dimensionless form or, equivalently, with Eq. (7) with the special choices $A = 1\ \mathrm{s}^{-1}$ and $\Delta x = 1$ m. That is, our unit of time is A^{-1} and the unit of length is the compartment width Δx. For notational convenience we will continue to write x, t, and ρ, with the understanding that these are now equivalent to the dimensionless quantities ξ, τ, and $\widetilde{\rho}$. We further stick to the values $B_R = 0.1$ and $B_L = 0.2$ just as in the previous sections.

IV. TWO-STEP PROCESS LEADING TO CLUSTERING

A. First step: Onset of the oscillatory pattern

As we saw in the Introduction, the transition from the uniform density profile to the clustered state is accompanied by two specific events: (i) the appearance of small oscillations near the end of the conveyor belt, and (ii) the moment when the oscillatory pattern covers the entire system with a constant amplitude. The first event signals the *start* of the transition and the second one the *conclusion*. In this section we will show how these two events can be analyzed and understood in the context of the partial differential equation (7). We start with the first.

Under steady flow conditions, when the time derivative $\partial\rho/\partial t$ is zero, Eq. (7) takes the form $0 = -P(n)\partial\rho/\partial x + \partial/\partial x\{D(\rho)\partial\rho/\partial x\}$ with the obvious solution $\rho(x,t) = \rho_0$ (= const). Now, in order to study the stability of this horizontal density profile, we consider an arbitrary perturbation to it and see whether it grows or dies out. So we set

$$\rho(x,t) = \rho_0 + \varepsilon f(x,t), \tag{15}$$

with ε a small positive parameter and $f(x,t)$ a function at least twice differentiable with respect to x and at least once with respect to t, but otherwise arbitrary. Substituting this form in Eq. (7), and keeping only terms up to first order in ε of the Taylor expansion, we find that $f(x,t)$ must obey the following differential equation:

$$\frac{\partial f(x,t)}{\partial t} = -P(\rho_0)\frac{\partial f(x,t)}{\partial x} + D(\rho_0)\frac{\partial^2 f(x,t)}{\partial x^2}. \tag{16}$$

In this linearized equation the drift velocity and diffusion coefficient are constant. Their values, however, depend on ρ_0, see Eqs. (10) and (11), and this has the interesting consequence (as we will presently demonstrate) that the trivial solution $f(x,t) = 0$ becomes unstable above a certain threshold value of ρ_0.

To solve Eq. (16) we need one initial and two boundary conditions. As initial condition $f(x,0)$ we take a small random signal, with a different value at every Δx interval interpolated by third-order splines, fluctuating around zero with peak-to-peak amplitude 0.0002. This mimics an arbitrary random fluctuation and has the added advantage that it contains a wide range of Fourier modes. At the boundaries we take (inspired by the shape of the density profiles for the discrete system; see Fig. 3) the following Neumann boundary conditions:

$$\left.\frac{\partial f(x,t)}{\partial x}\right|_{x=0} = 0 \quad \text{and} \quad \left.\frac{\partial f(x,t)}{\partial x}\right|_{x=x_{\max}} = s_B, \tag{17}$$

where s_B denotes the (negative) slope the density profile has at its right end. In the discrete model, as we saw in Sec. II, the slope gets steeper for growing values of Q_{in} or, equivalently, for increasing density n_k. In the continuum model this slope assumes an active role: its value determines the shape of the rest of the profile, and thereby also the onset of the oscillations. So, whereas in the discrete system we simply observed that the slope s_B happened to be -0.75 when the first oscillations appeared, in the continuum version it is this slope (in combination with the critical density level) that triggers the oscillations.

As for any partial differential equation, if we would choose different boundary conditions we would find a different solution to Eq. (16). So at this point of our analysis we heavily lean on the observations from the discrete system; we *have* to if we want to reproduce the behavior of the discrete system.

In Fig. 6 we show the numerical solution of Eq. (16), with the initial and boundary conditions defined above, for several values of the slope s_B around the critical value. In order to facilitate the comparison with the discrete system of Figs. 3 and 4, we take the length of the conveyor belt to be equal to $x_{\max} = 155\Delta x$.

The successive values of ρ_0 and s_B represent increasing inflow rates Q_{in}. We start with $\rho_0 = 2.09$ and $s_B = -0.53$, corresponding to the relatively small inflow rate $Q_{\mathrm{in}} = 1.00$ of Fig. 3(a). The solution of the linearized equation (16) with these values is shown in Fig. 6(a). To be precise, we show the steady solution $\lim_{t\to\infty} f(x,t)$ superimposed on the constant ρ_0, i.e., the density profile $\lim_{t\to\infty} \rho(x,t)$. It is seen to correspond closely to the discrete density profile of Fig. 3(a).

The profile's instability to small ripplelike disturbances makes its appearance around the value $\rho_0 = 2.36$, when $s_B = -0.75$. The corresponding solution of Eq. (16) superimposed on ρ_0 is depicted in Fig. 6(b): It is here that we witness the birth of the first density oscillations.

The critical value of ρ_0 at which this birth takes place is of course not coincidental. First, $P(\rho_0)$ is very close to maximal [cf. Fig. 5(b), the maximum occurs at $\rho = 2.38$], which means—as we will show in Sec. V—that the tendency to create oscillations is at its peak. Second, the diffusion coefficient $D(\rho_0)$ has become quite small, meaning that any humps and depressions in the density profile are not so efficiently smoothed out anymore. Together these two circumstances are responsible for the emergence of the oscillatory pattern around $\rho_0 = 2.36$.

Finally, in Fig. 6(c) we go beyond the onset value and show the solution $\lim_{t\to\infty} f(x,t)$ (superimposed on ρ_0) for $\rho_0 =$

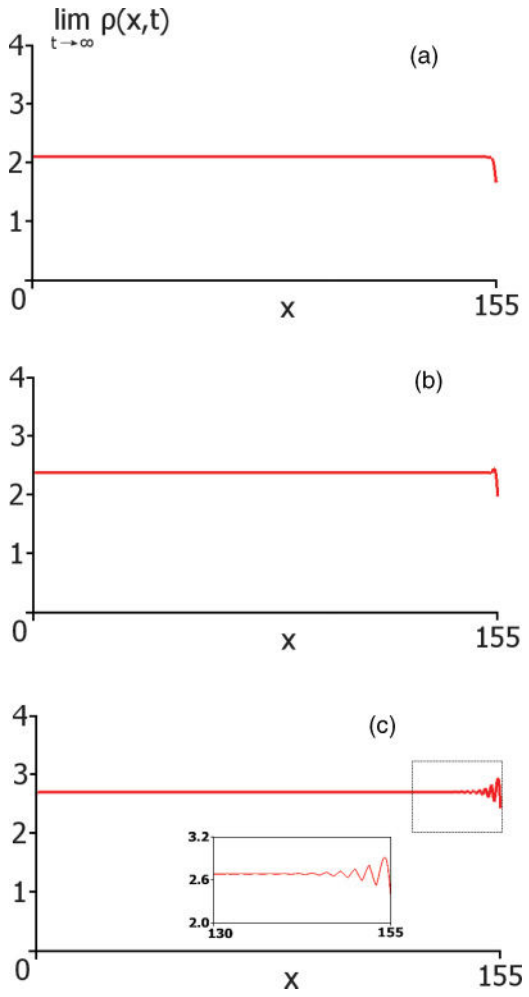

FIG. 6. (Color online) Birth of the oscillatory profile in the continuum model (cf. the corresponding stages for the discrete system in Fig. 3). (a) When the particle density is set to the relatively low value $\rho_0 = 2.09$, and the slope at the right end to $s_B = -0.53$, the solution of Eq. (16) with boundary condition (17) is zero throughout the system, with only a characteristic downward twist at the end. Superimposed on the constant level ρ_0 this gives the depicted density profile. (b) For $\rho_0 = 2.36$ and $s_B = -0.75$ the solution shows a tiny oscillation at the rightmost end. This is the first step toward clustering. (c) At $\rho_0 = 2.68$ and $s_B = -0.93$ the wavy pattern has expanded toward the left, with a clear periodicity of $2\Delta x$.

2.68 and $s_B = -0.93$. This is a near-perfect reconstruction of the discrete profile for $Q_{\text{in}} = 1.80$ in Fig. 3(b).

We see that, from all the Fourier modes present in the initial condition, the system selects the one with wavelength $2\Delta x$, and—thanks to the fact that we have identified Δx with the compartment width—this is just the same as in the discrete model, where the profile was found to be periodic with twice the compartment width [20]. In fact, even if we take an initial condition $f(x,0)$ from which the wavelength $2\Delta x$ is deliberately lacking, the system (by means of its boundary conditions) still produces this same oscillatory profile with wavelength $2\Delta x$. We note that this is the shortest wavelength the system can generate (given the discretization step Δx), indicating that the uniform density profile is primarily unstable for perturbations on the smallest possible length scale.

If we increase ρ_0 further [thereby making the diffusion coefficient $D(\rho_0)$ smaller and smaller, see Fig. 5(b)] and simultaneously let the slope s_B become steeper, we find that the oscillatory pattern expands toward the left. This mimics the behavior of the full system. Here, however, we go beyond the regime for which the linearized equation (16) was derived and one should return to the full Eq. (7).

The fact that the oscillatory profile of the discrete system with its two-compartment periodicity is reproduced so well by the continuum model, which is largely due to our identification of Δx with the compartment width, illustrates the importance of choosing a discretization step suited to the problem at hand. Besides, it justifies our choice of keeping only terms up to quadratic order in Δx in the Taylor expansion of Eq. (6). If the correspondence would have been less satisfactory, we would have been forced to include terms of higher order and study the (more involved) differential equation that emerges in that case.

B. Second step: Instability of the fully developed oscillatory pattern

We now come to the second step: the destabilization of the oscillatory profile and the birth of the cluster. In order to analyze this, we study small perturbations to the fully developed wavy pattern:

$$\rho(x,t) = \rho_{\text{cr}}(x) + \varepsilon g(x,t), \tag{18}$$

where $\rho_{\text{cr}}(x)$ is given by [see Fig. 7(a)]

$$\rho_{\text{cr}}(x) = \rho_{0,\text{cr}} - \alpha \cos(2\pi x/\lambda), \tag{19}$$

with wavelength $\lambda = 2\Delta x$, amplitude $\alpha = 0.2500$, and average value $\rho_{0,\text{cr}} = 2.7534$. The perturbation $g(x,t)$ is an arbitrary function at least twice differentiable with respect to x and once with respect to t. Inserting the above form Eq. (18) into Eq. (7), the terms of order ε in the Taylor series give the following partial differential equation for $g(x,t)$:

$$\begin{aligned}\frac{\partial g(x,t)}{\partial t} &= -P[\rho_{\text{cr}}(x)]\frac{\partial g(x,t)}{\partial x} - \left.\frac{\partial P}{\partial \rho}\right|_{\rho_{\text{cr}}(x)} \frac{\partial \rho_{\text{cr}}(x)}{\partial x} g(x,t) \\ &\quad + \frac{\partial}{\partial x}\left\{ D[\rho_{\text{cr}}(x)]\frac{\partial g(x,t)}{\partial x} + \left.\frac{\partial D}{\partial \rho}\right|_{\rho_{\text{cr}}(x)} \frac{\partial \rho_{\text{cr}}(x)}{\partial x} g(x,t)\right\}.\end{aligned} \tag{20}$$

Solving this equation requires one initial condition and two boundary conditions. For the initial condition $g(x,0)$ we again take a small random fluctuation around zero with amplitude 0.0001. The boundary conditions now are

$$\left.\frac{\partial g(x,t)}{\partial x}\right|_{x=0} = s_A \quad \text{and} \quad \left.\frac{\partial g(x,t)}{\partial x}\right|_{x=x_{\max}} = s_B = -1.00. \tag{21}$$

The negative slope s_B corresponds to the familiar density drop at the end of the system. Its value at the critical stage when the cluster is born is found (from the discrete system) to be around -1.00; in the present analysis we keep it fixed. The new feature is the slope s_A at the *entrance* of the system. In

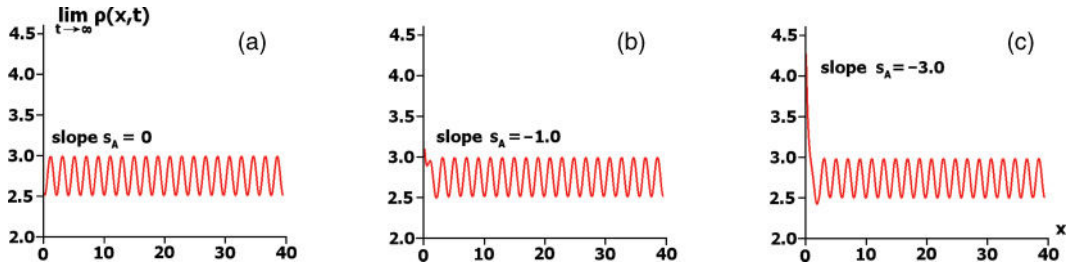

FIG. 7. (Color online) Birth of the cluster in the continuum model. (a) The uniform oscillatory density profile [Eq. (19)] at the brink of clustering. The slopes at the left and right boundaries are $s_A = 0$ and $s_B = -1.00$, respectively. Note that the latter boundary (at $x = 155\Delta x$) is not shown. (b) When the slope at the left end is set to $s_A = -1.00$ (keeping $s_B = -1.00$), the solution of Eq. (20) with boundary conditions (21) is zero throughout the system with only two characteristic twists at the ends. Here we show this solution superimposed on the uniform oscillation of plot (a) on the interval $x = 0$ to $x = 40\Delta x$. The first signs of cluster formation at the left end are clearly visible. (c) If we allow the slope s_A to become steeper, here to $s_A = -3.00$, the cluster at the entrance of the system grows accordingly.

the situation of the uniform oscillatory profile (19) this slope is still zero, but when we force the system beyond this point, the slope s_A must acquire a negative value. This represents the fact that the inflow rate is now larger than what the system can handle, creating a density surplus at $x = 0$, which must necessarily connect to the rest of the profile via a negative slope.

In Figs. 7(b) and 7(c) we depict the solution of Eq. (20) for two successive values of s_A beyond the critical point. We start with $s_A = -1.00$, which represents the first stages of the cluster formation. Indeed, the small random initial fluctuation $g(x,0)$ rapidly develops a sharp peak (followed by a small dip) at $x = 0$ and an equally sharp drop (preceded by a small hump) at $x = 155\Delta x$, while everywhere else it relaxes to zero. The superposition of the steady state $\lim_{t\to\infty} g(x,t)$ and $\rho_{\rm cr}(x)$ is depicted in Fig. 7(b).

In Fig. 7(c) we repeat the same procedure, but now with $s_A = -3.00$. This new value of s_A (demanding a steeper slope at the entrance of the system) corresponds to the next stage in the time evolution of the growing cluster. As we see in Fig. 8, the height of the cluster in the first compartment grows linearly with the value of $|s_A|$.

We could go on increasing the value of $|s_A|$, and witness the peak in $x = 0$ become higher and higher, but we rather stop here. The stages described above are meant to correspond to the transition from Figs. 4(a) to 4(b) and no further. When the density profile deviates too much from the uniformly oscillating profile, the linearized equation (20) loses its validity

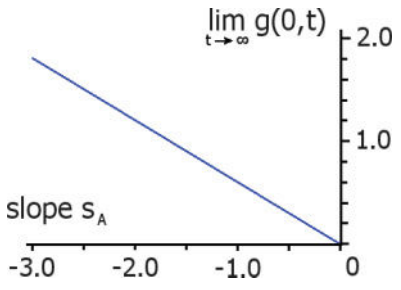

FIG. 8. (Color online) The value of $g(0,t)$ in the limit $t \to \infty$ as a function of the slope s_A. The plot shows that the two are linearly related. The value of $\lim_{t\to\infty} g(0,t)$ superimposed on $\rho_{\rm cr}(0)$ gives the height of the cluster at $x = 0$, as in Fig. 7.

and one should return to the full system given by Eq. (7). To be precise, in order to reproduce the further growth of the cluster at the entrance of the system [as observed in Figs. 4(c)–4(e)] one should study the full Eq. (7) and let the slope at $x = 0$ gradually become steeper with increasing density $\rho(0,t)$. Simultaneously, to reproduce the depletion of the rest of the system (between cluster and exit), also the boundary condition at $x = x_{\rm max}$ should be adjusted continuously. Getting everything right requires a delicate balancing between the two boundary conditions, which is doable but will not be pursued here.

V. PHYSICAL INTERPRETATION

The key for explaining the clustering transition in the continuum model is the interplay between the drift and diffusion terms in Eq. (7), with their nonconstant coefficients $P(\rho)$ and $D(\rho)$. It is instructive to first consider the drift term separately. To this end we take the reduced equation

$$\frac{\partial\rho(x,t)}{\partial t} = -P(\rho)\frac{\partial\rho(x,t)}{\partial x}, \tag{22}$$

which is an example of a nonlinear advection equation, describing the transport of material by a medium whose velocity $P(\rho)$ depends on the density of that same material. If $P(\rho)$ would depend linearly on ρ, Eq. (22) would take the form of the well-known inviscid Burgers equation. For our granular transport system, however, $P(\rho)$ is a more complicated function of ρ [see Eq. (10)] which only becomes linear in the limit $B_{R,L}\rho^2 \to 0$.

Let us solve Eq. (22) with an initial condition that mimics the uniform profile of Fig. 3(a) [see also Fig. 6(a)], with a density level $\rho = 2.09$ that is well below the value 2.36 at which [according to Fig. 6(b)] the first oscillations appear. The boundary condition we impose (note that only one boundary condition is needed in this case) is that the derivative $\partial\rho/\partial x|_{x=x_{\rm max}}$ has the same negative value $s_B = -0.53$ as we used before in Eq. (17). The result is shown in the upper row of Fig. 9. Within 50 time steps the initially flat profile is turned into an oscillatory pattern that extends over the whole length of the system. The drift term alone is responsible for this behavior.

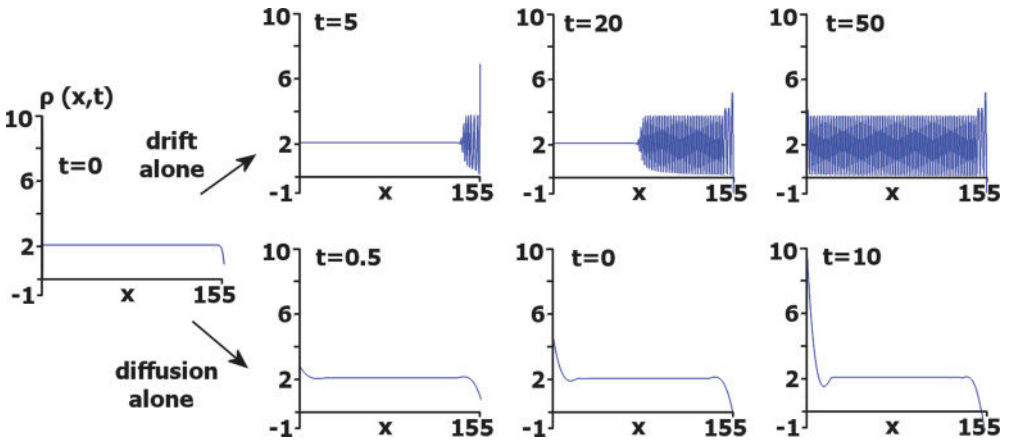

FIG. 9. (Color online) Starting from a flat and relatively low density profile, we study the influence of the drift and diffusion terms separately. The figures in the top row show the numerical solution of Eq. (22), which contains only the drift term, revealing a strong tendency to form waves. The figures in the bottom row depict the solution of Eq. (23), containing only the diffusion term, and here we witness a tendency to form a cluster at the left side of the system.

Similarly, we may study the pure effect of the diffusion term by means of the reduced equation

$$\frac{\partial \rho(x,t)}{\partial t} = \frac{\partial}{\partial x}\left\{ D(\rho)\frac{\partial \rho(x,t)}{\partial x}\right\}. \tag{23}$$

This is an example of a nonlinear heat equation [33] and closely related to the Kardar-Parisi-Zhang equation, which is used to model the spontaneous roughening of crystal surfaces in solid state physics [34–36].

To solve it, we choose the same initial profile as above. At the boundaries (we now need two boundary conditions) we require $\partial\rho/\partial x|_{x=0} = s_A = -1.00$ and $\partial\rho/\partial x|_{x=x_{\max}} = s_B = -0.53$. In the bottom row of Fig. 9 we see that, by the action of the diffusion alone (assisted by the boundary condition at $x = 0$), the homogeneous profile develops a peak at the left side of the system. Evidently, the density has at some stage exceeded the critical level for which the diffusion coefficient ceases to be positive and turns into antidiffusion. Density differences are then no longer smoothed out, but amplified. This is the continuum analog of clustering.

So we see that the drift term is responsible for the formation of density oscillations, whereas the diffusion term is the one that causes the clustering at the entrance of the system. The overall behavior of Eq. (7) is an interplay between these two effects. The whole sequence of events leading to the cluster formation can be understood from Fig. 10, which shows $P(\rho)$ (drift velocity) and $D(\rho)$ (diffusion coefficient) side by side.

At low density levels the diffusion coefficient is positive, and much larger than the drift velocity, and therefore washes away any attempts of the term $-P(\rho)\partial\rho/\partial x$ to generate waves; see the inset in the lower left corner of Fig. 10.

For increasing ρ the dominance gradually changes. In Fig. 10 we see that $P(\rho)$ becomes larger than $D(\rho)$ for $\rho \approx 2$. The diffusion is still positive but quickly loses strength and at some point is simply unable to suppress the oscillations anymore. This point comes at $\rho \approx 2.36$, when $P(\rho)$ is near its maximum value. This is the stage when the first density oscillations appear at the end of the conveyor belt in the continuum model. When we increase the inflow further, the oscillations quickly conquer the entire system. Meanwhile, the diffusion coefficient is still decreasing but it is preparing a remarkable comeback.

This happens at $\rho = 2.75$, when $D(\rho)$ becomes negative. And it is at this point that the competition between drift and diffusion suddenly turns into a collaboration, because the antidiffusion (the tendency to enhance density differences) finds an ideal starting point in the oscillatory pattern caused by the drift term. Thanks to this, the clustering sets in without delay as soon as $D(\rho)$ becomes negative, thus completing the clustering transition.

Looking at the transition from beginning to end, it is worthwhile to highlight the fact that it *starts at the rear end of the system* (with the first appearance of the density

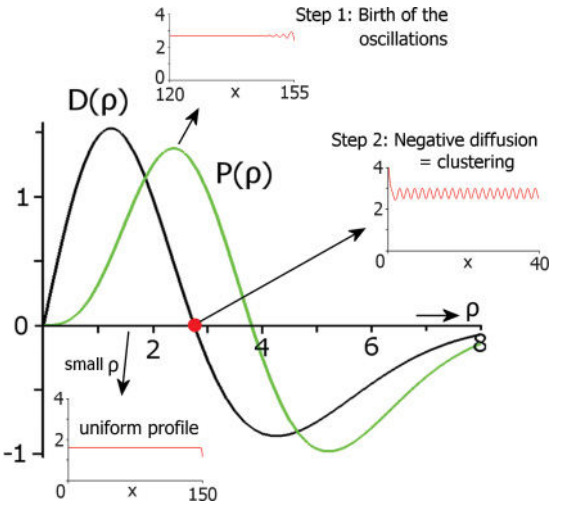

FIG. 10. (Color online) The diffusion coefficient $D(\rho)$ and the drift velocity $P(\rho)$ side by side. At small values of ρ the diffusion dominates, resulting in a smooth density profile. At larger ρ the drift term takes over and induces the characteristic density oscillations. At a slightly higher value of ρ, the diffusion coefficient $D(\rho)$ becomes negative, turning the diffusion into antidiffusion: it is at this point that the clustering sets in.

oscillations) and is *completed at the front* with the formation of the cluster. This is intimately related to the boundary conditions at respectively $x = x_{\max}$ and $x = 0$.

In the first step, the boundary condition at the entrance is trivial ($\partial\rho/\partial x|_{x=0} = s_A = 0$) so nothing special happens here. Only at the other end of the system do we have a boundary condition that changes (the slope s_B at $x = x_{\max}$ becomes steeper) as the amount of material $\int \rho(x,t)dx$ contained in the system grows; naturally then it is *here* that the first signs of the clustering transition appear. This happens at the critical density level 2.36 when $s_B = -0.75$; see Fig. 6(b).

Vice versa, when we arrive at the second step nothing special happens at $x = x_{\max}$. This time the slope at $x = 0$ (s_A) plays the leading part, simply by acquiring a nonzero value when the oscillatory profile reaches the entrance of the system. As a result, the density level at the entrance is locally made to rise, marking the birth of the cluster.

In the continuum model we tune the values of $s_A = \partial\rho/\partial x|_{x=0}$ and $s_B = \partial\rho/\partial x|_{x=x_{\max}}$ by hand, so in a sense we are triggering the critical events ourselves. However, the chosen values faithfully reproduce the discrete system where the same things happen spontaneously. It is precisely this—to reproduce and explain the observations of the discrete system—that has been the aim of the continuum model all along.

VI. CONCLUSION

By translating the original discrete system into the language of continuous media, the present work has brought to light the two physical mechanisms (drift and diffusion) that are at work in the granular transport system. It has also elucidated the intricate interplay between these two mechanisms, leading to the formation of a cluster at the entrance of the system and the breakdown of the particle flow. The sequence of events is summarized in Fig. 10.

The same method of translating a discrete dynamical system into a continuum model may be applied to other systems of interest, such as chains of oscillators, pedestrian traffic, or the flow of vehicles on highways [13,14]. As we have seen, the crucial point in order to ensure that the continuum model will be perfectly tailored to capture all the details of the dynamics is to choose the step size in the Taylor expansion (Δx) to be the same as the size of the discrete elements of the original system. In our transport system this was the compartment width. In traffic modeling it would be the size of a typical car (plus some extra space to avoid collisions), which is in the order of $\Delta x = 7.5$ meters [37]. A larger step size also generates a continuum model, of course, but will not be capable of reproducing all the local features of the system. A smaller step size is not advisable either, since it may generate artificial structures at sizes smaller than the elements of the discrete system.

The method is especially suited for the study of critical points, where we can focus on a specific set of parameters. Following the entire evolution of the system for changing parameters (the inflow Q in the present paper) is more cumbersome, since any parameter change must be translated into a corresponding change in the boundary conditions.

One of our main results was that the clustering transition is directly related to the change in sign of the diffusion coefficient $D(\rho)$ when ρ exceeds a certain threshold value: When the density in any compartment happens to exceed this threshold, the regular diffusion is locally reversed into antidiffusion. This means that material is drawn from the surrounding compartments and a cluster is formed. The other compartments, which have a smaller density and hence a diffusion coefficient that is still positive, are drained empty.

A transition from overall diffusive behavior to (local) antidiffusion is by no means a rare phenomenon. It can be found in a host of systems that are prone to localization and clustering. One example is the diffusion-antidiffusion phase transition in stochastic processes that are attractive at low temperatures and dispersive at high temperatures [38]. Another typical example is the spontaneous formation of a "phantom" traffic jam when the local vehicle density exceeds a critical threshold value (around 30 veh/km per lane, see [13,14] and references therein). Finally we mention that space- and time-dependent diffusion coefficients, which may locally become negative, appear also in Hamiltonian systems where regular and chaotic orbits co-exist. For instance, the coherent motion of charged particles in plasmas has recently been described in terms of a drift-diffusion equation very similar to the one derived in the present paper [39].

ACKNOWLEDGMENTS

This work is part of the research programme of the European Complexity-NET project "Complex Matter," which is financially supported by the Greek General Secretariat for Research and Technology. We thank Professor D. Ghikas, Professor T. Bountis, Professor D. van der Meer, and Professor Y. Kominis for insightful comments on an early version of this work. The photo inset of Fig. 1 shows a demonstration model from the Physics of Fluids Group of the University of Twente, The Netherlands, and we take the opportunity to thank our colleagues for sharing it with us.

[1] S. B. Savage and K. Hutter, J. Fluid Mech. **199**, 177 (1989).
[2] Y. Forterre and O. Pouliquen, Annu. Rev. Fluid. Mech. **40**, 1 (2008).
[3] J. M. N. T. Gray, M. Wieland, and K. Hutter, Proc. R. Soc. London, Ser. A **455**, 1841 (1999).
[4] I. Zuriguel, J. M. N. T. Gray, J. Peixinho, and T. Mullin, Phys. Rev. E **73**, 061302 (2006).
[5] J. M. N. T. Gray and C. Ancey, J. Fluid Mech. **629**, 387 (2009).
[6] B. P. B. Hoomans, J. A. M. Kuipers, W. J. Briels, and W. P. M. van Swaaij, Chem. Eng. Sci. **51**, 99 (1996).
[7] H. Jaeger, S. Nagel, and R. Behringer, Rev. Mod. Phys. **68**, 1259 (1996).
[8] J. Duran, *Sand, Powders, and Grains: An Introduction to the Physics of Granular Materials* (Springer, New York, 2000).

[9] J. T. Jenkins and S. B. Savage, J. Fluid Mech. **130**, 187 (1983); J. T. Jenkins and M. W. Richman, Phys. Fluids **28**, 3485 (1985).
[10] M. C. Cross and P. C. Hohenberg, Rev. Mod. Phys. **65**, 851 (1993).
[11] I. Goldhirsch, Annu. Rev. Fluid Mech. **35**, 297 (2003).
[12] I. S. Aranson and L. S. Tsimring, Rev. Mod. Phys. **78**, 641 (2006).
[13] D. Chowdhury, L. Santen, and A. Schadschneider, Phys. Rep. **329**, 199 (2000).
[14] D. Helbing, Rev. Mod. Phys. **73**, 1067 (2001).
[15] A. John, A. Schadschneider, D. Chowdhury, and K. Nishinari, Phys. Rev. Lett. **102**, 108001 (2009).
[16] J. Eggers, Phys. Rev. Lett. **83**, 5322 (1999).
[17] K. van der Weele, D. van der Meer, M. Versluis, and D. Lohse, Europhys. Lett. **53**, 328 (2001).
[18] G. Kanellopoulos and K. van der Weele, *Critical Flow of Granular Matter on a Conveyor Belt*, AIP Conf. Proc. No. 1076 edited by M. Robnik and V. G. Romanovski (AIP, Melville, NY, 2008), pp. 112–121.
[19] K. van der Weele, G. Kanellopoulos, C. Tsiavos, and D. van der Meer, Phys. Rev. E **80**, 011305 (2009).
[20] G. Kanellopoulos and K. van der Weele, Int. J. Bifurcation Chaos **21**, 2305 (2011).
[21] D. van der Meer, Ph.D. thesis, University of Twente, Enschede, The Netherlands, 2004.
[22] D. van der Meer, K. van der Weele, P. Reimann, and D. Lohse, J. Stat. Mech.: Theor. Exp. (2007) P07021.
[23] K. van der Weele, Contemp. Phys. **49**, 157 (2008).
[24] R. Mikkelsen, K. van der Weele, D. van der Meer, M. van Hecke, and D. Lohse, Phys. Rev. E **71**, 041302 (2005).
[25] A. Lipowski and M. Droz, Phys. Rev. E **65**, 031307 (2002); **66**, 016118 (2002).
[26] F. Coppex, M. Droz, and A. Lipowski, Phys. Rev. E **66**, 011305 (2002).
[27] I. Bena, F. Coppex, M. Droz, and A. Lipowski, Phys. Rev. Lett. **91**, 160602 (2003).
[28] The critical value given in the text applies to conveyor belts with infinitely many compartments ($K \to \infty$), whereas for any finite number of compartments the particle flow will survive for slightly higher values of Q [20]. For $K = 155$, however, the critical value $Q_{\rm cr}(K)$ is practically equal to the critical value for $K \to \infty$.
[29] D. van der Meer, K. van der Weele, and D. Lohse, Phys. Rev. Lett. **88**, 174302 (2002).
[30] H. Risken, *The Fokker-Planck Equation: Methods of Solution and Applications*, 2nd ed. (Springer, Berlin, 1989).
[31] D. Frank, *Nonlinear Fokker-Planck Equations: Fundamentals and Applications* (Springer, Berlin, 2005).
[32] N. G. van Kampen, *Stochastic Processes in Physics and Chemistry*, 3rd ed. (North-Holland, Elsevier, Amsterdam, 2007).
[33] A. D. Polyanin and V. F. Zaitsev, *Handbook of Nonlinear Partial Differential Equations* (Chapman and Hall/CRC, Boca Raton, FL, 2003).
[34] M. Kardar, G. Parisi, and Y. C. Zhang, Phys. Rev. Lett. **56**, 889 (1986).
[35] T. Sasamoto and H. Spohn, Phys. Rev. Lett. **104**, 230602 (2010).
[36] P. Calabrese and P. LeDoussal, Phys. Rev. Lett. **106**, 250603 (2011).
[37] K. Nagel and M. Schreckenberg, J. Phys. I **2**, 2221 (1992).
[38] H. Bebie and J.-P. Marchand, Physica D **46**, 342 (1990).
[39] Y. Kominis, A. K. Ram, and K. Hizanidis, Phys. Rev. Lett. **104**, 235001 (2010).